Understanding junction breakdown in multicrystalline solar cells

Otwin Breitenstein[1], Jan Bauer[1,a], Karsten Bothe[2], Wolfram Kwapil[3], Dominik Lausch[4], Uwe Rau[5], Jan Schmidt[2], Matthias Schneemann[5], Martin Schubert[3], Jan-Martin Wagner[1,b], Wilhelm Warta[3]

[1]*Max Planck Institute of Microstructure Physics, Weinberg 2, D-06120 Halle, Germany*

[2]*Institute for Solar Energy Research Hameln/Emmerthal (ISFH), Am Ohrberg 1, D-31860 Emmerthal, Germany*

[3]*Fraunhofer Institute for Solar Energy Systems (ISE), Heidenhofstraße 2, D-79110 Freiburg, Germany*

[4]*Fraunhofer Center for Silicon Photovoltaics (CSP), Walter-Hülse-Straße 1, D-06120 Halle, Germany*

[5]*IEF5-Photovoltaik, Forschungszentrum Jülich, 52425 Jülich, Germany*

Abstract: Extensive investigations on industrial multicrystalline silicon solar cells have shown that, for standard 1 Ωcm material, acid-etched texturization, and in absence of strong ohmic shunts, there are three different types of breakdown appearing in different reverse bias ranges. Between -4 and -9 V there is early breakdown (type 1), which is due to Al contamination of the surface. Between -9 and -13 V defect-induced breakdown (type 2) dominates, which is due to metal-containing (most probably iron silicide) precipitates lying within recombination-active grain boundaries. Beyond -13 V we may find in addition avalanche breakdown (type 3) at etch pits, which is characterized by a steep slope of the *I-V* characteristic, avalanche carrier multiplication by impact ionization, and a negative temperature coefficient of the reverse current. If instead of acid-etching alkaline-etching is used, all these breakdown classes also appear, but their onset voltage is enlarged by several volts. Also for cells made from upgraded metallurgical grade (UMG) material these classes can be distinguished. However, due to the higher net doping concentration of this material, their onset voltage is considerably reduced here.

I. Introduction

Since the electric potentials between the cells in a string of a solar module are floating, the individual cell biases strongly depend on the individual cell characteristics. If e.g. one cell in a module should be broken or shadowed and therefore generates a considerably reduced current, this cell may become reverse-biased by the other cells in the string by up to -13 V. If in this cell a large reverse current flows in one site, this site may heat up excessively (generation of hot spots), which may lead to thermal destruction of the module. Therefore reverse currents in solar cells are a serious reliability issue and their origin must be well understood. The most frequent and

[a] Now with CaliSolar GmbH, Magnusstraße 11, D-12489 Berlin

[b] Now with Christian-Albrechts-Universität zu Kiel, Institut für Materialwissenschaft, Kaiserstraße 2, D-24143 Kiel

actually trivial sources of reverse currents in solar cells are ohmic shunts. The origins of ohmic shunts are well-known. They may be caused by incomplete opening of the edge, by cracks, by Al-contamination of the emitter, or they may be material-induced [1]. In the latter case they are due to n-conducting SiC filaments crossing the bulk, which exist preferably in grain boundaries of material from the upper part of the block [2]. The present contribution will not deal with these ohmic shunts but will concentrate on real junction breakdown processes. It will collect the most important results of several previous publications of the authors, which all have been devoted to single aspects of the general breakdown behavior, together with previously unpublished results, to form a complete overview of the present knowledge of breakdown occurring in multicrystalline silicon solar cells.

II. Experimental

The results shown later in Sect. III are obtained on a few cells made industrially from adjacent wafers of standard solar-grade silicon material ($p \approx 1*10^{16}$ cm^{-3}) by using standard screen-printing technology with full-area Al back contact and acid-etched texturization. In Sect. IV the physical origin of the three dominating breakdown types found in Sect. III will be dealt with by using data of the same and other but equivalent cells. In Sect. V it will be reported how the results change if alkaline-etching or UMG material is used instead. All these investigations have been confirmed many times on cells from different producers, leading in all cases basically to the same results. Thus, it can be guaranteed that the results shown here are typical for today's standard solar cell technology.

Besides dark current-voltage (*I-V*) characteristic measurements, most of the results rely on lock-in thermography (LIT [3]) under reverse bias and on electroluminescence (EL) imaging under forward [4] and reverse bias [5, 6]. LIT imaging allows to detect all kinds of reverse currents (ohmic and junction breakdown) quantitatively. The local current density is given by the local LIT signal divided by the applied bias. The basic constraint of LIT is its limited spatial resolution, which is basically due to lateral heat diffusion. For the investigation of breakdown phenomena in solar cells, special LIT techniques have been developed for imaging different physical properties of breakdown sites quantitatively [7]. By evaluating LIT images taken in the dark (DLIT) at different temperatures and biases, images of the temperature coefficient (TC, given in % current change per K) of the local currents and of the relative slope of the local *I-V* characteristics (given in % current change per V) may be obtained. Since these parameters are normalized to the total current values, they are not influenced by the magnitude of the individual local breakdown currents but generally characterize the underlying breakdown mechanism. Finally, the presence of avalanche breakdown can be uniquely proven by quantitatively imaging the local avalanche multiplication factor (MF) of photo-generated carriers by applying a special illuminated LIT method (MF-ILIT [7]).

EL under forward bias relies on light generated by radiative recombination of electrons and holes in the bulk. The luminescence peaks at about 1100 nm and basically images the "internal voltage" in the bulk, which is strongly influenced by grown-in recombination-active crystal defects. Hence, the dark lines visible in forward-bias EL images are basically decorated grain boundaries (random, twin, or small-angle grain boundaries, which are rows of dislocations). EL under reverse bias (called in the following ReBEL [8]), on the other hand, relies on acceleration or scattering of carriers in high electric fields. It is attributed to bremsstrahlung [9] or to hot carrier recombination [10] and shows a wide-band spectrum including contributions in the visible range. The spatial resolution of reverse-bias EL imaging is considerably better than that of LIT or

forward-bias EL [6, 8]. Stronger ohmic shunts locally short-circuit the p-n junction. Therefore they cannot be seen by reverse-bias EL imaging since there is no sufficiently high electric field in these positions.

III. General breakdown behavior

A solar cell with a bulk doping concentration of 10^{16} cm^{-3} should show under reverse bias a saturation current in the order of 10^{-10} A/cm^2 and break down by avalanche not before -60 V [11]. In real solar cells, even in absence of ohmic shunts, the reverse characteristic at low bias is always linear (ohmic), it becomes super-linear at a few volts reverse bias, and significant breakdown may appear already at a reverse bias beyond -10 V. Fig. 1 shows a typical reverse characteristic of a cell without ohmic shunts in linear drawing at two temperatures (a) and at room temperature in half-logarithmic drawing (b). We see that, at a bias below -13 V, the current increases with increasing temperature [positive temperature coefficient (TC), see arrow], and beyond -13 V it decreases with increasing temperature (negative TC, see arrow). Below -13 V the characteristic is essentially exponential with a medium slope, but beyond -13 V the current steeply increases. Already this result points to the fact that obviously in different bias ranges different breakdown mechanisms dominate.

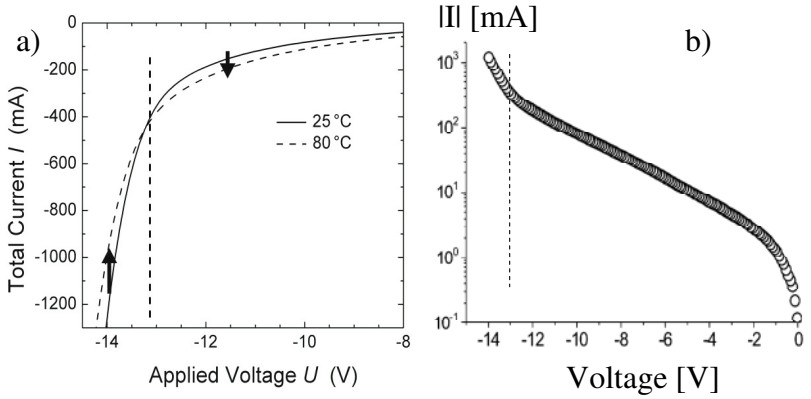

Fig. 1: Reverse current-voltage characteristic (a) in linear drawing at two temperatures and (b) at room temperature in half-logarithmic drawing [13]

It can be expected that these different mechanisms are active in different regions of the cells. Therefore DLIT and ReBEL have been used to localize the corresponding breakdown sites. In Fig. 2 a typical cell is imaged at room temperature under three different reverse biases by DLIT (a-c), by ReBEL (d-f), and by forward-bias EL (g). All images are differently scaled to show the most important items, the scaling limits are given in the caption. Generally, the reverse-bias EL images show a better spatial resolution than the DLIT images, as expected. The general correlation between DLIT and EL is very good, except for the images taken at -8 V. In the following, we will call all breakdown sites occurring (for our typical samples) below -9 V as "early breakdown" or "type 1" breakdown sites [12]. This breakdown type is often found in edge regions and partly also in the cell area. There is no visible correlation to the forward-bias EL image (g). We have observed that some of these early breakdown sites, which are visible in DLIT, are not visible in ReBEL. The reason for this discrepancy will be discussed in Sect. IV (A). Starting from -9 V more and more breakdown sites successively appear. Only at -12 to -13 V these sites show a clear correlation to recombination-active grown-in crystal defects, see Fig. 2 (b), (e), and (g). We will call this breakdown type "defect-induced" or "type 2" breakdown. The physical origin of this breakdown type will be discussed in Sect. IV (B). If the reverse bias is further increased to above -13 V, a third breakdown type may become dominant, which we call

"avalanche" or "type 3" breakdown. The origin of this type will be discussed in detail in Sect. IV (C). It will be discussed in Sect. V that all these three different breakdown types are also present in alkaline-etched and in UMG-based solar cells, except that they exist there in different bias ranges.

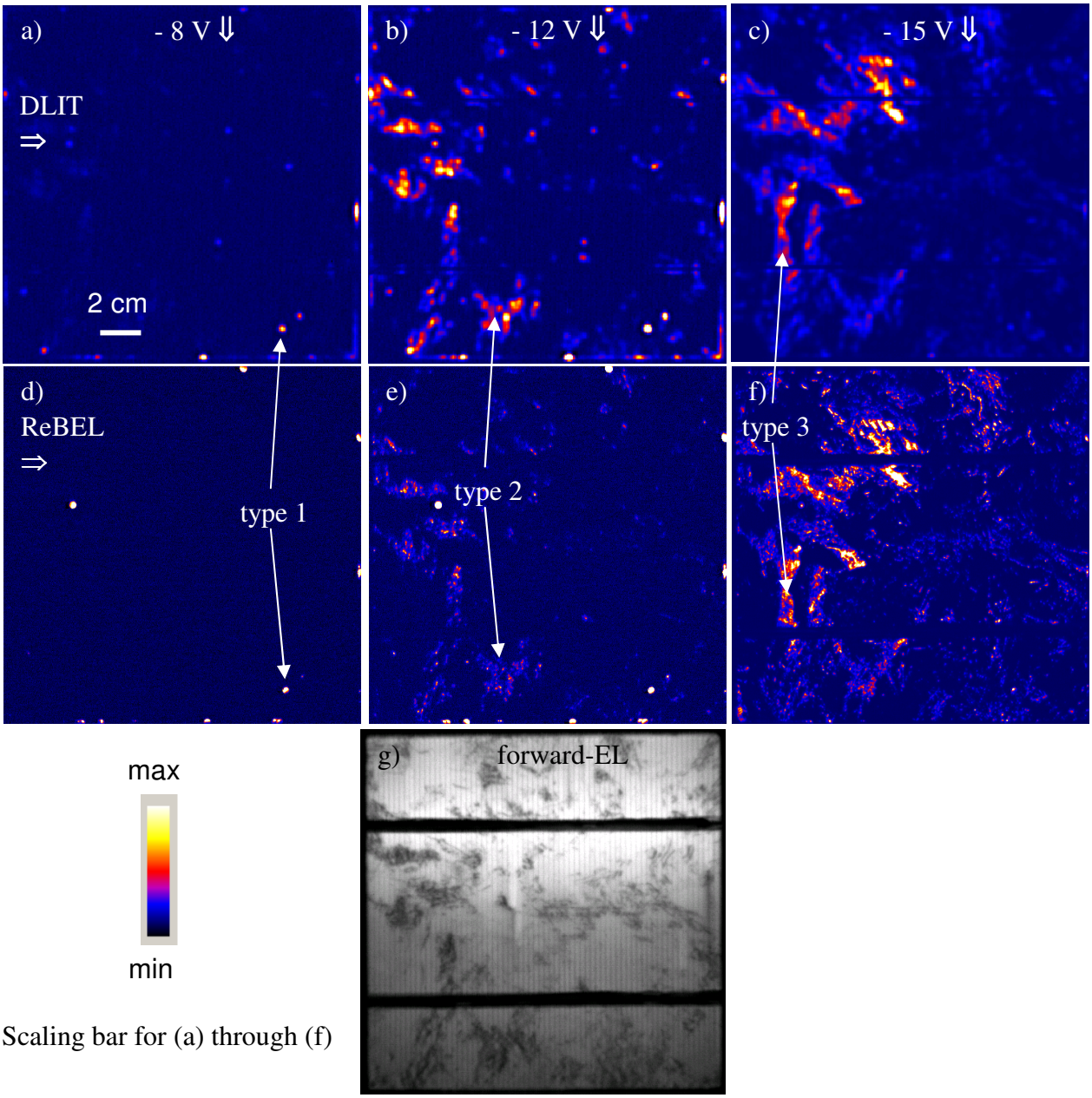

Fig. 2: (a) DLIT at -8 V; max. 6 mK, (b) DLIT at -12 V; max. 6 mK, c) DLIT at -15 V; max. 150 mK, (d) ReBEL at -8,2 V, max. 100 a.u., (e) ReBEL at -12 V, max. 100 a.u., (f) ReBEL at -15 V, max. 1000 a.u., (g) EL (+ 0,6 V) 1100 nm, a.u.

The different breakdown types may exist intermixed side-by-side, so that they can hardly be separated by DLIT or even ReBEL. In favorite cases, however, in certain regions one breakdown mechanism dominates. In Fig. 2 such typical regions are indicated for the different breakdown

types. It is interesting to note that not only type 1 but also type 3 is not correlated to the recombination-active crystal defects visible in Fig. 2 (g). Fig. 3 (a) shows measured *I-V* characteristics of small pieces of solar cells which have been cut out so that each piece is dominated by only one breakdown type [13]. It is visible that for type 1 the current increases nearly linearly. Only beyond -13 V a steeper increase occurs, which may be due to the unintended presence of other breakdown types in this piece. For type 2 the current increases exponentially with a medium slope. For type 3 until -13 V only a weak current flows (which is probably due to other sources, e.g. the sawed edge leading to an ohmic contribution [13]), but beyond -13 V the current steeply increases. The same behavior is visible in Fig. 3 (b) where data of the local ReBEL intensity (full symbols) and of the local current density measured by DLIT (i.e. the local DLIT signal divided by the applied bias [3]; open symbols and roman numbers for the different breakdown types) are drawn in the positions of separately appearing breakdown types as a function of reverse bias [14]. For each breakdown type two different measurements have been done (at different positions), labeled as a and b in Fig. 3 (b). All data are normalized to their value at -20 V. This figure generally confirms the results of the direct current measurement in (a). The relation between ReBEL intensity and breakdown current depends on breakdown type, but (b) proves that the ReBEL signal is at least for each breakdown type roughly proportional to the mean breakdown current density, see also Fig. 5 below. Obviously breakdown type 1 is characterized by a linear or only slightly super-linear characteristic, type 2 by an exponential one with medium slope, and type 3 by a steep current increase above a certain threshold voltage.

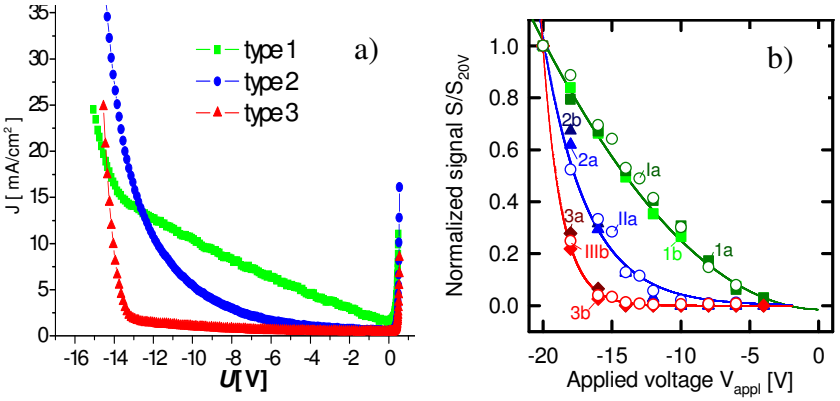

Fig. 3: (a) Reverse *I-V* characteristics of solar cell pieces containing only one dominating breakdown type [13], (b) ReBEL signal (filled symbols) and DLIT current density (open symbols and roman numbers) for two sites (a and b) of each breakdown type [14]

IV Breakdown mechanisms

A. Early breakdown

This breakdown type can be observed already at -5 V and below. As mentioned before, it may or may not be connected with light emission in ReBEL. It has been found recently [15] that this breakdown type is connected with Al particles at the surface, which reside on the wafer before the deposition of the silicon nitride antireflection layer and before emitter contacting. Fig. 4 (a) shows a microscopic ReBEL image and the corresponding topography image (b) of a particle at the surface, together with the SEM image (c) and an EDX mapping of the Al line (d) of this particle. A similar result was already shown in [1], and also [16] points to Al contamination. It is well-known that Al as a p-dopant may overcompensate the n^+-emitter if the cell is heated up, e.g. during contact firing. Then the area below an Al particle will become p^+-conducting and will be electrically in contact with the p-type base of the cell. The p^+-n^+ junction between the emitter and the Al-doped silicon yields a highly doped p-n junction. Now it depends on the size of the

particle and on the amount of Al doping below the particle whether this will become a high-doped p-n junction, a weak ohmic shunt, or a strong ohmic shunt. A highly doped p-n junction may break down already at a few volts reverse bias by internal field emission (Zener effect), thereby emitting light [17]. If breakdown occurs only in microscopic spots (see light spots in Fig. 4 a), there should be a high series resistance to the breakdown sites. Therefore, for increasing reverse bias the series resistance will limit the current increase, which explains the observed linear characteristic. If the p-doping concentration below the Al particle exceeds a certain level, the p^+-n^+ junction will become an ohmic tunnel junction. It has been discussed already at the end of Sect. II that a stronger ohmic shunt should prevent the formation of local high electric fields that are responsible for the ReBEL light emission. We believe that this is the case in those early breakdown sites which do not show ReBEL. However, if the ohmic shunt is very weak, a high field still may establish locally under reverse bias, again leading to a ReBEL signal.

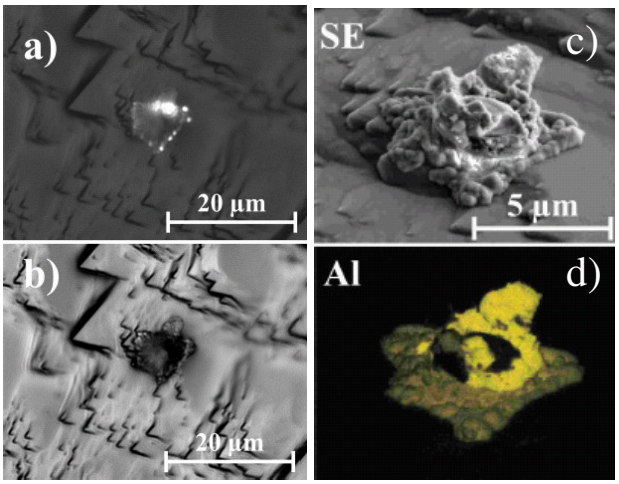

Fig. 4: (a) Microscopic ReBEL image and (b) surface topography (reflected light image) of a particle at the surface, (c) SEM (SE) image of this particle, (d) EDX mapping of the Al line [15]

B Defect-induced breakdown

It was shown already in Fig. 2 that the type-2 breakdown sites correlate with recombination-active crystal defects. This correlation is demonstrated in detail in Fig. 5, showing a high-resolution DLIT image (a, 0° image at -12 V, 222 Hz lock-in frequency), a forward bias EL image (b), a ReBEL image at -12 V (c) and (d) the superposition of (b) and (c) of a group of type-2 breakdown sites. It can be seen that all in DLIT visible breakdown sites are also visible in ReBEL (with one exception, see arrow), that the two signal heights are well correlating (hence the ReBEL signal is reflecting the magnitude of the breakdown current), and that all breakdown sites are lying on dark lines visible in forward bias EL (b). Similar results have been found by Usami et al. [17] and, with even better spatial resolution, by Lausch et al. [8]. Small deviations in the position may be explained by grain boundaries lying inclined to the surface. The exception (arrow) is an ohmic shunt, which has been proven by bias-dependent DLIT investigations to show a linear *I-V* characteristic down to zero volts.

Since the dark lines in Fig. 5 (b) show a constant contrast over their length, but the breakdown sites are very local, the recombination-active defect states themselves should not be responsible for the breakdown. Fig. 6 (a) shows a DLIT image made at -9 V of a cell made from material of a small-scale casting experiment. The upper and the lower edge were close to the edge of the crucible used. This crucible was of the same type as industrial crucibles, just being considerably smaller. It is well known that iron is the dominant impurity diffusing from the crucible walls into the edge zone of cast material [18]. Therefore, the increased breakdown site density at the top and

at the bottom of Fig. 6 (a) is certainly due to an increased Fe contamination in these regions. Direct evidence of Fe precipitation was found recently by micro X-ray fluorescence (µ-XRF) investigations at breakdown sites [20]. Fig. 6 (b) shows a SEM image of a position containing two breakdown sites in grain boundaries (see insets) together with µ-XRF mappings of iron in these two sites (c). Obviously, the type-2 breakdown is originated from iron-containing precipitates lying within Fe-contaminated grain boundaries. These precipitates consist most probably of $FeSi_2$, which is metallic-like. If a small $FeSi_2$ precipitate crosses the p-n junction, it yields an ohmic contact to the highly doped emitter and a Schottky contact to the base. This Schottky contact has a significantly lower barrier height than the p-n junction and therefore breaks down earlier. Thus, this breakdown mechanism is most probably Schottky diode breakdown, which is due to field emission or thermionic field emission [21]. Maybe there are also other precipitate types involved in this mechanism (by TEM, besides Fe- also Cu-, Sn-, and Ca-containing precipitates have been found), and also a tip effect at the small precipitates at the base side should play a role for reducing the breakdown voltage. This explains why the onset voltage of type-2 breakdown sites spreads over an extended reverse bias range from about -9 V to -13 V. Note that this breakdown type also exists on flat surfaces, where it shows somewhat higher breakdown voltages [8].

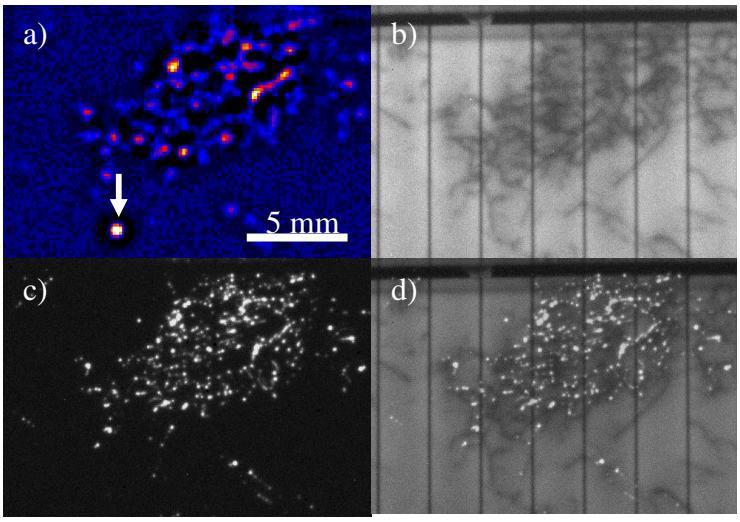

Fig. 5: (a) High resolution DLIT image, (b) forward-bias EL image, (c) ReBEL image, and (d) superposition of (b) and (c) of a group of type 2 breakdown sites. The arrow in (a) points to an ohmic shunt

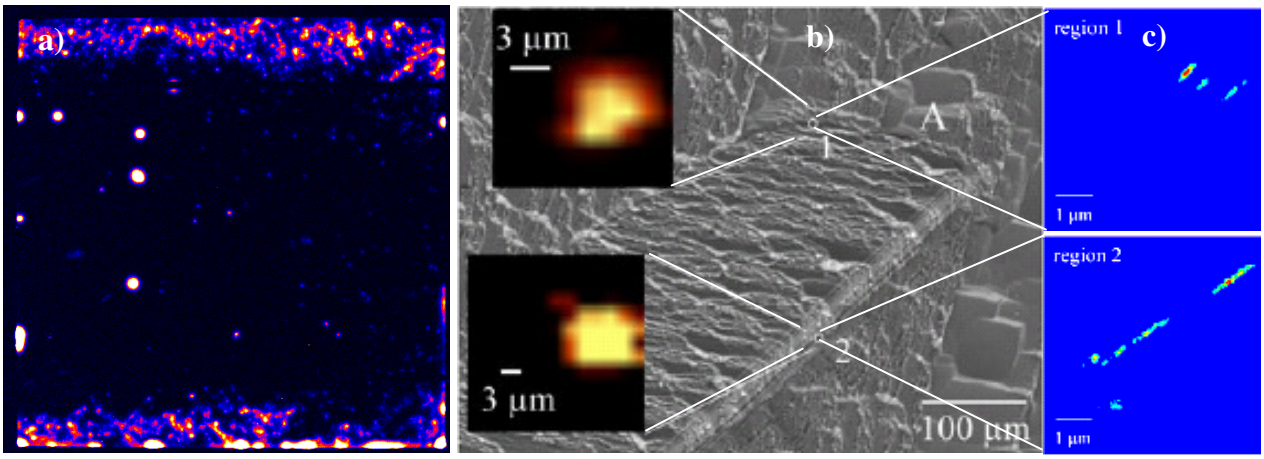

Fig. 6: (a) DLIT image of type-2 breakdown (at -9 V), upper and lower edge region contaminated by iron, (b) SEM image of a region containing two type-2 breakdown sites (ReBEL, see insets), (c) µ-XRF mapping of iron in both breakdown sites [20]

It had been mentioned already in Sect. III that the type-2 breakdown sites are appearing with increasing reverse bias one after the other in an extended reverse bias range. The question arises whether the individual *I-V* characteristics of single breakdown sites are exponential, linear, or even saturation-type? In all cases the exponential *I-V* characteristic measured for these breakdown sites shown in Fig. 3 could be explained. This problem has recently been solved on alkaline-etched solar cells by applying bias-dependent high spatial resolution ReBEL investigations [22]. Note that in these cells the onset voltages are higher than in the acid-etched cells shown until now, see [8]. As Fig. 7 shows, the single breakdown sites show different onset voltages and nearly linear intensity-voltage characteristics. Fig. 5 has shown that the ReBEL intensity at least correlates with the breakdown current. Actually, any junction breakdown itself should show a strongly super-linear characteristic. However, since these breakdown sites are of sub-micron size, they are coupled to the terminals of the cell by a relatively high series resistance, which linearizes the individual characteristics. The even slightly sub-linear type of the intensity-voltage characteristics can probably be explained by the increasing sample temperature with increasing reverse bias, which may lead to a reduced optical quantum efficiency. Obviously the exponential *I-V* characteristic establishes mainly by the appearance of new breakdown sites, as Fig. 7 (b) shows. Interestingly, the intensity-voltage characteristics of the breakdown sites showing a higher onset voltage are showing a lower slope, which is not understood yet.

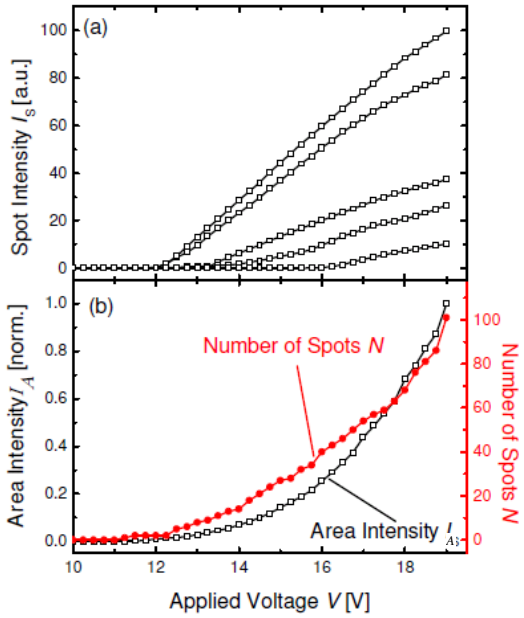

Fig. 7: (a) ReBEL intensity of different individual type-2 breakdown sites, (b) comparison of integrated area intensity and counted number of spots in a region in a alkaline-etched cell [22]

C. Avalanche breakdown

The acidic etching solution, which is used today for isotropic texturization of multicrystalline solar cells, actually is optimized not to lead to etch pits at crystal defects like dislocations. Nevertheless, in some regions etch pits may exist. It has been found that these etch pits are leading to avalanche-type breakdown [23]. This breakdown type is characterized by a steep (threshold-like) *I-V* characteristic and a negative temperature coefficient (TC) of the current, since the mean scattering energy of carriers in the field reduces with increasing temperature. Moreover, multiplication of light-induced carriers occurs only under avalanche conditions, which may be used as a proof of avalanche breakdown occurring. Fig. 8 shows images of the avalanche multiplication factor MF (a), of the TC (b), and of the slope (c), all measured at -15 V on the cell used for Fig. 2 by using special LIT methods [7]. In the position indicated by the arrows there is considerable avalanche carrier multiplication, a clearly negative TC and a high slope of the

breakdown current. At -12 V, in this position was no breakdown visible yet in Fig. 2 (b) and (e), and in Fig. 2 (g) there are no recombination-active crystal defects there.

By using lock-in EBIC (electron beam-induced current) under -15 V reverse bias, microscopic carrier multiplication sites (microplasma) could be found in the positions of etch pits, e.g. that indicated by the arrows in Fig. 9 [23]. The cross-sectional TEM image (c) shows that the tip radius is in the order of 20 nm. Since the p-n junction is expected to lie 300 nm below the surface, at the tip of the etch pit it should be bowl-shaped with a radius of 300 nm. Sze and Gibbons [11] have shown that under this condition the breakdown voltage for 10^{16} cm^{-3} material reduces from -60 V to -13 V, which is exactly the avalanche threshold measured by us. Thus, at least for acid-etched cells, the hard breakdown type 3 appearing beyond -13 V is due to avalanche occurring at etch pits. Since also these breakdown sites are microscopic, their individual characteristics should also be linearized by a high series resistance as shown for type 2 sites in Fig. 6a. However, in contrast to the type-2 sites, all type-3 sites show the same breakdown voltage, since for all of them the geometry and the doping concentration are the same. Therefore, close to the onset voltage, the averaged slope of the breakdown current in type-3 breakdown sites is much higher than for sites with type-2 breakdown. Note also the considerably higher local density of type-3 sites (see Fig. 9) compared to type-2 sites (see Fig. 5).

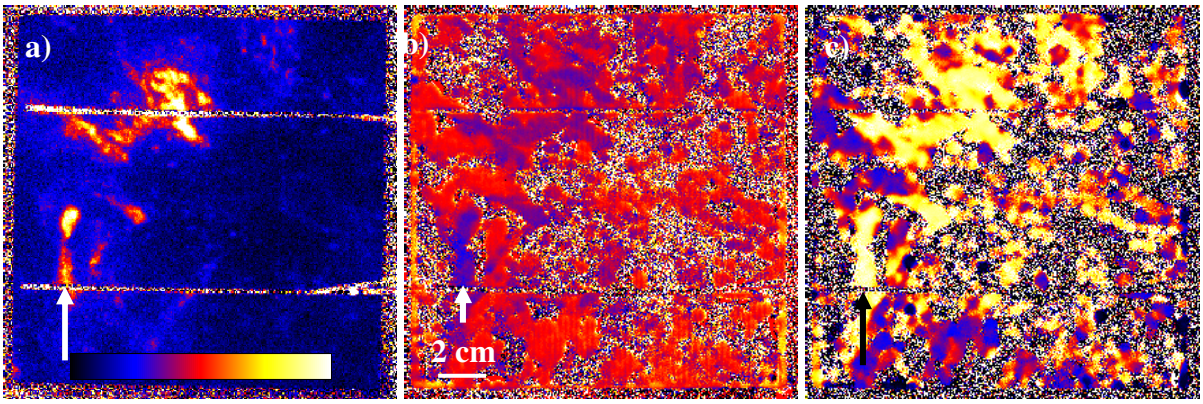

Fig. 8: (a) Avalanche multiplication factor (0 to 3), (b) temperature coefficient (-5 to +5 %/K), and (c) relative slope of the current (0 to 200 %/V) of the cell used for Fig. 2, all measured at -15 V at room temperature. The arrows point to a position where pure avalanche breakdown occurs.

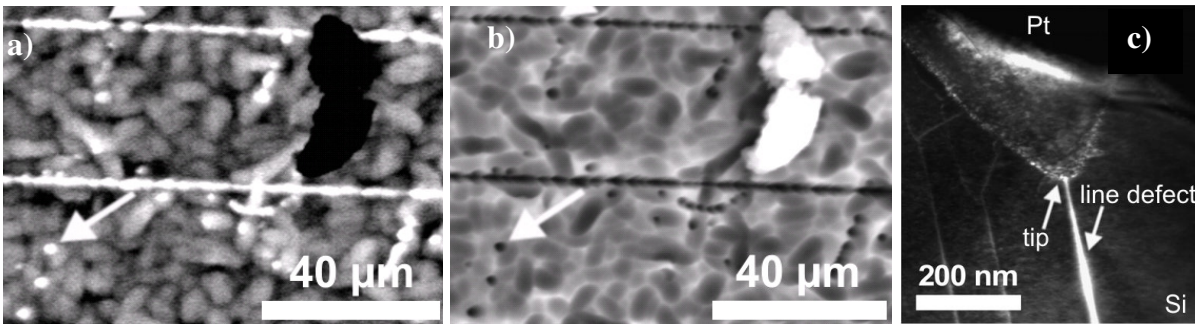

Fig. 9: (a) Lock-in EBIC image at -15 V showing microplasma (arrow) in a type-3 breakdown site, (b) SE image, (c) TEM cross section image of the tip of an etch pit [23]

The question arises where these etch pits come from. They are certainly not due to simple dislocations, since the dislocation density in this material is much higher than the etch pit density, and also in Fig. 9 (c) some more dislocations are visible which do not lead to etch pits. Recent TEM investigations on such an etch pit have shown that the corresponding line defect is lying in a 10 nm wide 180° twin lamella extended in $[11\bar{1}]$-orientation [24]. This is the reason why these etch pits are often lying in rows. The line defects are dislocations in $[1\bar{1}0]$ direction embedded in one of the twin boundaries, which are split by about 3 nm and seem to be heavily decorated at one side, probably by carbon. The origin of these defects and the reason why they lead to etch pits is not clear yet.

V Breakdown in alkaline-etched and UMG cells

Systematic investigations have shown that at least type-1 and type-2 breakdown exists also in alkaline-etched cells, except that there, for a given net doping concentration, the threshold voltages are about 2 - 4 Volts higher. This was nicely shown for type-2 breakdown sites by Lausch et al. [8], see Fig. 10. The difference in the breakdown voltages can probably be related to the higher roughness of acid-etched surfaces, which lead to higher field strengths. The investigation of avalanche effects in alkaline-etched cells is still underway.

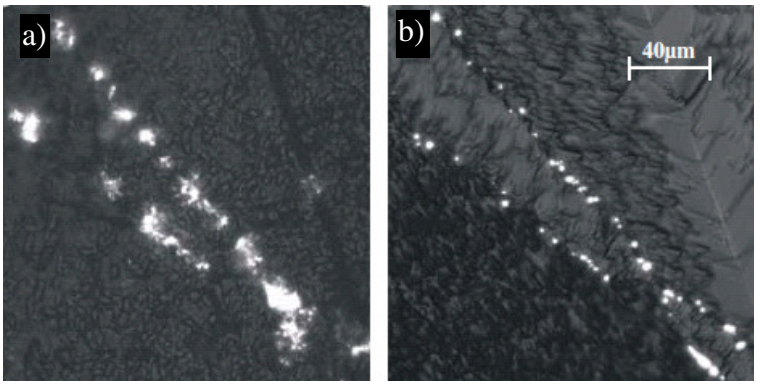

Fig. 10: ReBEL images of Typ-2 breakdown in cells made from adjacent wafers, (a) at -13 V on an acid-etched, and (b) at -17 V on an alkaline-etched cell [8]

It had been suspected in the past that UMG material should be heavily polluted by metallic impurities. However, it has turned out that metals are no serious efficiency-limiting factor in UMG cells. Obviously the metal concentration in this material is low enough that the standard cell process, which may tolerate a relatively high metal contamination, is not negatively affected yet. However, it can be expected that residual metal contamination influences the breakdown behavior of UMG cells. Another problem of UMG material is the high residual B and P concentration, which leads to a high net doping concentration in the lower part of the ingot and decreasing net doping concentration towards the top, where the conductivity changes to n-type [25]. It is well known that the net doping concentration strongly influences the breakdown behavior [26]. Fig. 6 (a) also proves that Fe contamination increases the type-2 breakdown current. The question now is: Which of the two factors (metal contamination or net doping concentration) dominate the breakdown behavior of UMG cells? This can be checked e.g. by comparing the breakdown currents of cells from different heights in a UMG block. From bottom to top the metal concentration should increase due to the low segregation coefficient of all metals, but the net doping concentration decreases since P has a lower segregation coefficient than B. Hence, if the breakdown current increases towards the top, the influence of the metal

contamination dominates, and if it decreases the net doping concentration influence dominates. Fig. 11 shows that for standard material the influence of contamination is dominating, but for UMG material the influence of the net doping concentration dominates. Note that for this judgment the current contribution which is strongly increasing towards high reverse bias is decisive, since the slowly rising current at low reverse bias is governed by ohmic shunts.

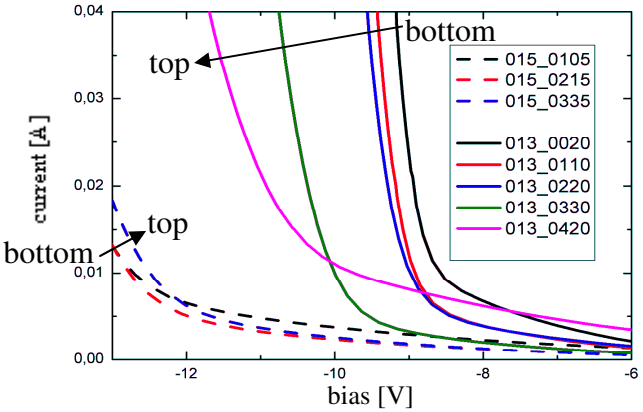

Fig. 11: Reverse characteristics of cells from different block heights (given by the second number in legend) of standard material (#015, dashed lines) and UMG material (#013, full lines)

In a thorough analysis recently published by Kwapil et al. [27], breakdown voltages of cells made from standard and UMG material with various net doping concentrations were measured and compared by two different criteria, see Fig. 12. In this graph the UMG cells (open symbols) smoothly fit to the standard cells (full symbols), which proves that the high net doping concentration is the main reason for early breakdown in UMG material.

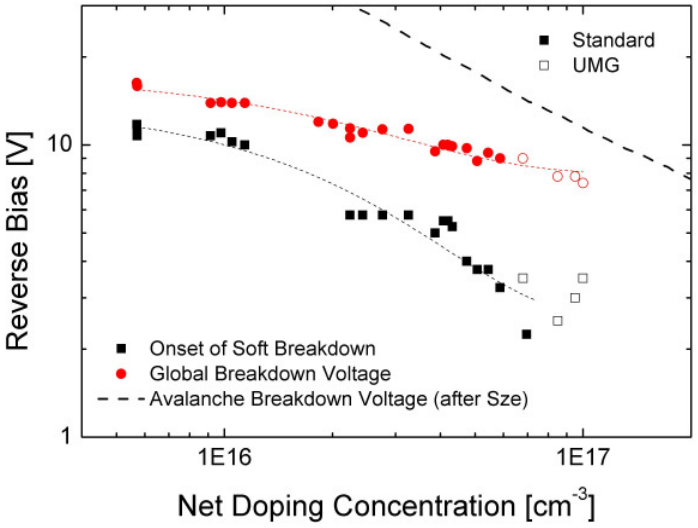

Fig. 12: Different representations of the diode breakdown voltage versus the net doping concentration in the base of standard and UMG solar cells [27]. The circles depict the voltage of maximum curvature in the global reverse characteristics while the rectangles show the approximate reverse voltage at which first breakdown ReBEL emission is detected at soft breakdown sites (thin dashed lines serve as guides to the eye). For comparison, the thick dashed line represents the expected avalanche breakdown voltage for defect-free one-sided abrupt pn junctions [11].

VI Conclusions

It has been demonstrated here that there are three clearly distinguishable breakdown mechanisms in multicrystalline solar cells: Early breakdown caused by Al-contamination (type 1), defect-induced breakdown caused by $FeSi_2$ or other precipitates lying in grain boundaries (type 2), and avalanche breakdown caused by etch pits (type 3). The question is which type of breakdown is most dangerous? Note that the investigations shown here have been made on cells without strong ohmic shunts. The type-1 "breakdown" sites are at best weak ohmic shunts, so they are not harmful at all. Nevertheless, Al contamination at the surface has to be avoided, since

heavy Al contamination leads to strong ohmic shunts, which also may lead to hot spots under reverse bias. Ohmic hot spots may also be caused by incomplete opening of the edge, by cracks, or by grown-in SiC filaments [1]. The defect-induced breakdown type 2 is often the dominating one in the interesting bias range up to -13 V. However, as Figs. 2 (b) and (e) show, there are usually many of these breakdown sites distributed across the area. As Fig. 7 shows, the individual breakdown currents are series resistance limited, high breakdown currents only establish by a large number of breakdown sites. Hence, even if the type-2 breakdown current is large, it should not easily lead to dangerous hot spots, since the heat distributes across the whole cell area and the local density of the breakdown sites is low. This is not the case anymore for type-3 (avalanche) breakdown. We have observed that these avalanche sites may cover only a small fraction of the area with a high local density of breakdown sites, and beyond a certain reverse bias the avalanche breakdown dominates due to its high slope. Thus, if the net doping concentration is high enough that significant avalanche breakdown occurs in the interesting bias range up to -13 V, this breakdown type may become as dangerous as are strong ohmic shunts. Therefore it should be interesting to further investigate the generation of these special etch pits and maybe to avoid their formation.

This work was supported by the BMU project 0327650 "SolarFocus". The authors are grateful to H. Blumtritt, N. Zakharov, and U. Hlawatsch (Halle), to A. Lotnyk (Kiel) for experimental cooperation.

References

[1] O. Breitenstein, J.P. Rakotoniaina, M.H. Al Rifai, M. Werner: "Shunt types in crystalline silicon solar cells", Prog. Photovolt.: Res. Appl. **12**, 529 (2004)

[2] J. Bauer, O. Breitenstein, J.P. Rakotoniaina: "Electronic activity of SiC precipitates in multicrystalline solar cells", phys. stat. sol. (a) **204**, 2190 (2007)

[3] O. Breitenstein, M. Langenkamp: "Lock-in Thermography - Basics and Use for Functional Diagnostics of Electronic Components", Springer (Berlin/Heidelberg/New York) 2003

[4] T. Fuyuki, H. Kondo, T. Yamazaki, Y. Takahashi, Y. Uraoka, Appl. Phys. Lett. **86**, 262108 (2005)

[5] R. Newman, Phys. Rev. **100**, 700 (1955)

[6] M. Kasemann, W. Kwapil, M.C. Schubert, H. Habenicht, B. Walter, M. The, S. Kontermann, S. Rein, O. Breitenstein, J. Bauer, A. Lotnyk, B. Michl, H. Nagel, A. Schütt, J. Carstensen, H. Föll, T. Trupke, Y. Augarten, H. Kampwerth, R.A. Bardos, S. Pingel, J. Berghold, W. Warta, S.W. Glunz: Spatially resolved silicon solar cell characterization using infrared imaging methods", Proc. 33rd IEEE Photovoltaic Specialists Conference, San Diego 2008, #148, DOI 10.1109/PVSC.2008.4922478

[7] O. Breitenstein, J. Bauer, J.-M. Wagner, A. Lotnyk: "Imaging physical parameters of pre-breakdown sites by lock-in thermography techniques", Prog. Photovolt: Res. Appl. **16**, 679 (2008)

[8] D. Lausch, K. Petter, H. v. Wenckstern, M. Grundmann: "Correlation of pre-breakdown sites and bulk defects in multicrystalline silicon solar cells", phys. stat. sol. RRL **3**, 70 (2009)

[9] T. Figielski, A. Torun: "On the origin of light emitted from reverse biased p-n junctions", in Proc. 6th Int. Conf Phys. Semicond. London, Pergamon, 1962, pp. 863-868

[10] A.G. Chynoweth, K.G. McKay: "Photon emission from avalanche breakdown in silicon", Phys. Rev. **102**, 369 (1956)

[11] S.M. Sze, G. Gibbons: "Effect of Junction Curvature on Breakdown Voltage in Semiconductors", Solid-State Electronics **9**, 831 (1966)

[12] W. Kwapil, M. Kasemann, P. Gundel, M.C. Schubert, W. Warta, P. Bronsveld, G. Coletti: "Diode breakdown related to recombination active defects in block-cast multicrystalline silicon solar cells", J. Appl. Phys. **106**, 063530 (2009)
[13] J. Bauer: "The origins of non-ideal current-voltage characteristics of solar cells", Ph.D. thesis 12/2009 at Martin Luther University Halle-Wittenberg, http://digital.bibliothek.uni-halle.de/hs/urn/urn:nbn:de:gbv:3:4-1951
[14] K. Bothe, K. Ramspeck, D. Hinken, C. Schinke, J. Schmidt, S. Herlufsen, R. Brendel, J. Bauer, J.-M. Wagner, N. Zakharov, O. Breitenstein: "Luminescence emission from forward- and reverse-biased multicrystalline silicon solar cells", J. Appl. Phys. **106**, 104510 (2009)
[15] D. Lausch, K. Petter, R. Bakowskie, C. Czekalla, J. Lenzner, H. v. Wenckstern, M. Grundmann: "Identification of Pre-Breakdown Mechanism of Silicon Solar Cells at Low Reverse Voltages", submitted to APL
[16] J.W. Bishop: "Microplasma breakdown and hot-spots in silicon solar cells", Solar Cells **26**, 335 (1989)
[17] A.G. Chynoweth, K.G. McKay: "Internal field emission in silicon p-n junctions", Phys. Rev. **106**, 418 (1957)
[18] N. Usami, K. Kutsukake, K. Fujiwara, I. Yonenaga, K. Nakajima: "Structural origin of a cluster of bright spots in reverse bias electroluminescence image of solar cells based on Si multicrystals", Appl. Phys. Express **1**, 075001 (2008)
[19] T. Uberg Nærland, L. Arnberg, A. Holt: "Origin of the low carrier lifetime edge zone in multicrystalline PV silicon", Prog. Photovolt: Res. Appl. **17**, 289 (2009)
[20] W. Kwapil, P. Gundel, M.C. Schubert, F.D. Heinz, W. Warta, E.R. Weber, A. Goetzberger, G. Martinez-Criado: "Observation of metal precipitates at breakdown sites in multicrystalline silicon solar cells", Appl. Phys. Lett. **95**, 232113 (2009)
[21] E.H. Rhoderick, R.H. Williams: "Metal-Semiconductor Contacts", Clarendon (Oxford) 1988
[22] M. Schneemann, A. Helbig, T. Kirchartz, R. Carius, U. Rau: "Reverse biased electroluminescence spectroscopy of crystalline silicon solar cells with high spatial resolution", accepted at Phys. Stat. Sol. (a)
[23] J. Bauer, J.-M. Wagner, A. Lotnyk, H. Blumtritt, B. Lim, J. Schmidt, O. Breitenstein: "Hot spots in multicrystalline silicon solar cells: avalanche breakdown due to etch pits", Phys. Stat. Sol. RRL **3,** 40 (2009)
[24] O. Breitenstein, J. Bauer, J.-M. Wagner, N. Zakharov, H. Blumtritt, A. Lotnyk, M. Kasemann, W. Kwapil, W. Warta: "Physical mechanisms of breakdown in multicrystalline silicon solar cells", accepted at IEEE Transactions on Electron Devices
[25] E. Enebakk, A.K. Soiland, J.T. Hakedal, R. Tronstad: "Dopant specification of compensated silicon for solar cells of equal efficiency and yield as standard solar cells", 3rd Int. Workshop on Crystalline Silicon Solar Cells, Trondheim (Norway), June 2009
[26] M. Wagner, B. Gründig-Wendrock, P. Palinginis, C. Knopf: "Shunts, diode breakdown and high reverse currents in multicrystalline silicon solar cells", Proc. 24th Eur. Photovoltaic Solar Energy Conference and Exhibition, Hamburg 2009, pp. 2028-2031
[27] W. Kwapil, M. Wagner, M. C. Schubert, W. Warta: „High net doping concentration responsible for critical diode breakdown behavior of upgraded metallurgical grade multicrystalline silicon solar cells", J. Appl. Phys., in print (2010)